

# Peak Analysis, Source Identification, and Gaussian Curve Fitting for Gamma Ray Spectroscopy

Jeff Lam, Ana McKiernan

*Department of Physics, Binghamton University*

May 12<sup>th</sup>, 2025

## Abstract

Gamma ray spectra for the radioactive sources Cs-137, Co-60, an unknown sample, and Na-22 were constructed using data collected from a scintillation detector. Scintillation materials luminesce under the presence of radioactivity, a consequence of the theories behind various modern physics phenomena, such as the photoelectric effect and Compton scattering. The specific scintillation detector used for gamma ray spectroscopy consisted of a thallium-doped sodium iodide (NaI(TL)) crystal hermetically sealed as a base, a photomultiplier tube to convert light from photoevents as weak signal to high-voltage outputs, and a digibase controller to organize each output into “channels”— histogram bins that represent different orders of energy levels. Various categorical peaks were considered, mainly the typical photopeaks amongst others such as backscatters, Compton edges, and annihilation. After developing Python code to help identify the appropriate channel number corresponding to the location of each photopeaks, a calibration curve was fitted using weighted linear-least squares fitting when additionally given the known energy levels of these photopeaks for Cs-137 and Co-60. The result is a calibration curve of the form  $\hat{y} = 0.1759x + 12.6326$ , allowing the performance of more advance experimental procedures on radiation sample. The first use case involved identifying an unlabeled radiation sample, which was successfully identified as Sb-125 using the same code that helped ascertain photopeak position channel number, and the second use case involved some success in fitting Gaussian curves to various explainable peaks of Na-22, to which the qualitative goodness in its fit can be seen and accessed.

---

## 1 Introduction

Radiation detectors are used to determine the presence of radioactive materials and for possible identification of said material. Typically, isotopes of various heavy elements are the sources of radioactive materials, where the amount of the isotopes present is generally of interest. These “nuclear material” emits gamma radiation of typically a few hundred keV or less, X-rays via beta decay, and alpha radiation via alpha decay [1].

### 1.1 Gamma Ray Spectroscopy

The gamma ray radiation emitted by nuclear materials are characteristic of the source element, allowing the identification of the isotopes. Various instruments may be used to detect gamma ray radiation such as gas filled detectors, scintillation detectors, semiconductor detectors, *etc.* Of these, scintillation and semiconductor detectors are the most extensive, however they suffer setbacks including but not limited to being operable only for small radioactive samples and lower efficiency [2]. The experiments involved in this paper employ a scintillation detector for detecting these radiation signals— refer to sec-

tion 3.1 *Scintillation Detectors* for the working theories behind scintillation and section 3.2 *Apparatus* for the model and brand type used for the experiments.

## 2 Theory

There are three interactions that may occur within a scintillation material when gamma rays pass through: the photoelectric effect, Compton scattering, and annihilation due to pair production. There are also X-ray emissions that occurs as a result of (primarily) the photoelectric effect. Of the three events, the first two are nearly ubiquitous across all radioactive materials— annihilation may be seen in one of the samples where data was collected in this paper, Sodium-22 (Na-22).

### 2.1 The Photoelectric Effect

**Figure 1** showcases the underlying principle behind the photoelectric effect. As it can be seen, an incoming photon interacts with a bound electron within the  $K$ -shell, transferring nearly all of its energy to the particle, thereby becoming a photoelectron by breaking the binding energy tied to its orbit around the atom. Let  $E_\gamma$  be the energy of the incident ray,  $E_{\text{bind.}}$  be the binding energy of the target electron, and  $E_e$  be the energy of the photoelectron. Because of the nearly complete transfer of energy from the photon to the electron, the Law of Conservation of Energy may be applied to produce the equation

$$E_e = E_\gamma - E_{\text{bind.}}$$

If the bound electron's binding energy is small (*i.e.*, electrons orbiting with the  $K$ -shell of its atom), then all kinetic energy carried by the photon is converted to the photoelectron, *i.e.*,  $E_{\text{bind.}}$  is negligible.

For the bound electron knocked out of orbit that

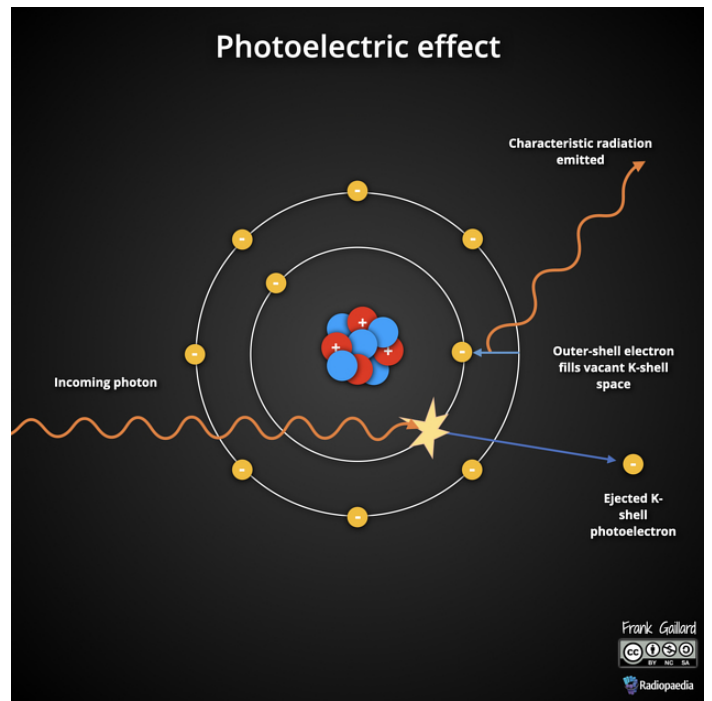


Figure 1: References diagram on the photoelectric effect [3]

was turned into a photoelectron, a neighboring electron orbiting within the next energy level, the  $L$ -shell, may replace the lost electron at its position, releasing some of the energy that it held when orbiting at the larger shell. These emissions are typically within the X-ray range, hence the term *X-ray emissions*. For certain radioactive isotopes, peaks picked up within the lower energy range may likely be these X-ray emissions.

### 2.2 Compton Scattering

**Figure 2** showcases an alternative interaction that may occur within scintillation: Compton scattering. In this scenario, a photon interacts with an electron in orbit of its parent atom, but unlike the photoelectric effect, its energy is not completely transferred over to create a photoelectron— instead, a recoil electron is produced, and the rest of the photon energy scatters away at some angle  $\theta$  from the recoil electron. In this scenario,  $E_\gamma$  only loses a portion of its kinetic energy— let  $E'_\gamma$  be the final kinetic energy carried by the scattering photon. The energy

relationship between the two can be written as

$$E'_\gamma = \frac{E_\gamma}{1 + 1.96 \text{ MeV} E_\gamma (1 - \cos(\theta))}$$

A derivation of this surprising result can be seen in **Appendix A: Derivation of the Compton Scattering Formula**, attached at the end of this paper.

For the special case that  $\theta = \frac{\pi}{2}$ ,  $\cos(\theta) = -1$ , and so the relationship can be further simplified to

$$E'_\gamma = \frac{E_\gamma}{1 + 3.91 \text{ MeV} E_\gamma}$$

Geometrically, this special case represents the scenario where both the scattering photon ray and recoil electron scatters antiparallel to each other. This interaction is therefore dubbed as “backscatter”<sup>†</sup>, and is yet another spectral feature that manifest as a peak during gamma ray spectroscopy.

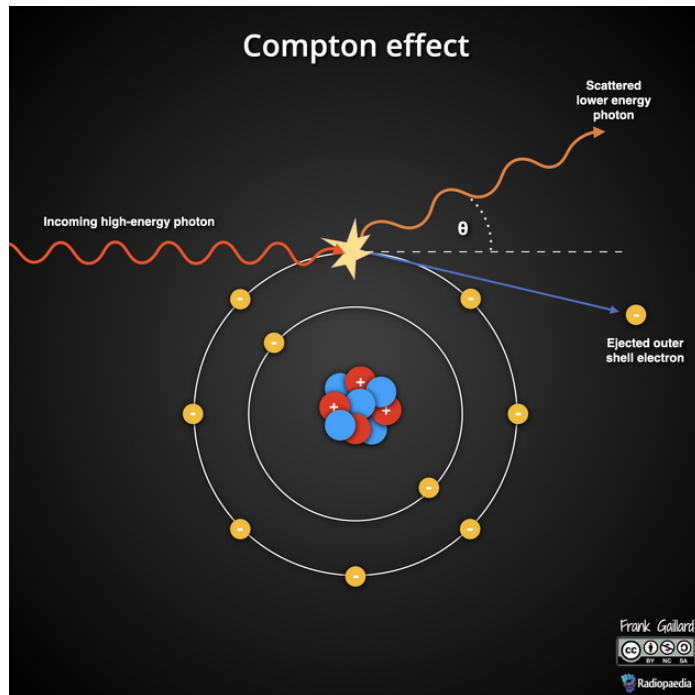


Figure 2: References diagram on the Compton effect [4]

<sup>†</sup>This, Compton scattering, and the photoelectric effect can be considered analogous to some classical mechanics interaction involving games of pool, for the various scenarios and results of a cue ball hitting an 8-ball from various conditions. For those familiar with pool/billiards terminology involving shot types, the backscatter interaction may be compared to a “draw shot”, the Compton scattering compared to an angled shot, and the photoelectric effect compared to the “stopped shot”.

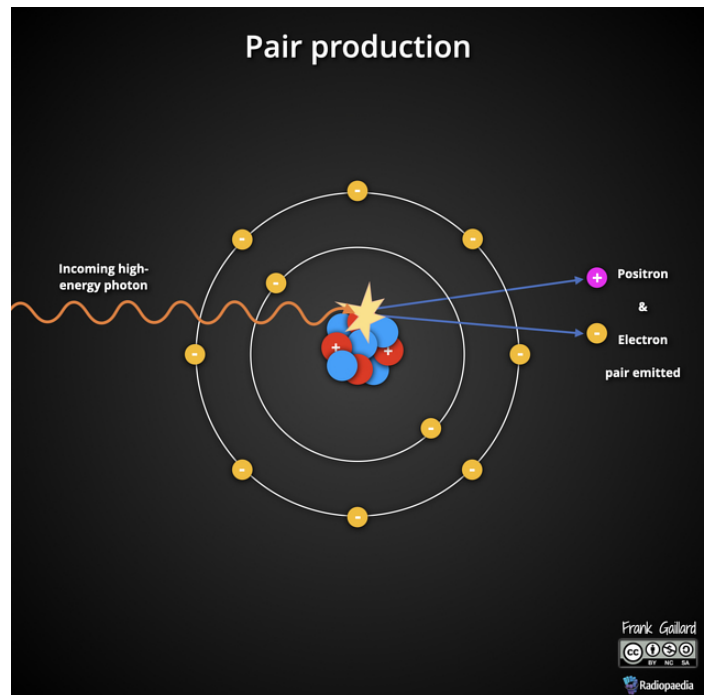


Figure 3: References diagram on pair production and annihilation [5]

### 2.3 Pair Production and Annihilation

**Figure 3** showcases one more scenario that may occur when gamma rays passes through (specifically) matter. If a gamma ray holding a kinetic energy at least greater than or equal to twice of that of an electron’s resting energy ( $\approx 511 \text{ keV}$ ), and if the ray passes through the nucleus of an atom, then it may convert into an electron, or more formally a *beta particle* ( $\beta^-$ ). But according to the Law of Conservation of Energy and Conservation of Momentum, an *anti-particle* is also created, holding the same but opposite charge of the electron and scattering at an equal angle opposite of the normal between it and the propagating beta particle. This anti-particle is dubbed the *positron* ( $\beta^+$ ).

Though the produced beta particle ( $\gamma \rightarrow \beta^- + \beta^+$ ) scatters away from the interaction, the positron being anti-matter nearly always interact with a

neighboring electron, annihilating each other (hence the term “annihilation”) and producing two other gamma rays that scatters opposite of each other as well.

### 3 Methods

#### 3.1 Scintillation Detectors

Scintillation detectors rely on scintillation materials— materials that luminesce under the presence of high-energy rays near the X-ray portion of the electromagnetic spectrum. Every gamma ray that passes through scintillation materials produces a light pulse, and each light pulse can be thought of as an individual “event”, thereby producing signals that may be processed. These signals, however, by themselves are too weak to be detected, and so in order to properly detect them a process called photomultiplication helps amplify these signals as high voltage outputs. These high voltage outputs then may be digitally logged by a computer software

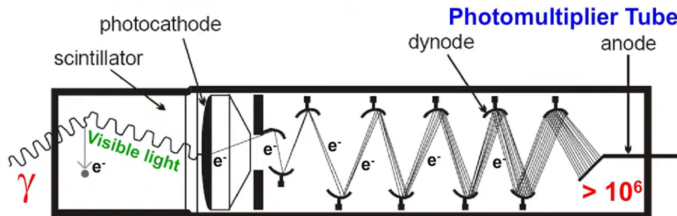


Figure 4: Snipped screenshot of [6] showcasing the process of photomultiplication.

**Figure 4** is a snipped screenshot of a reference, showcasing the steps of photomultiplication. Photomultiplication takes place in a PhotoMultiplier Tube (PMT), where the mechanism of the process is done. Incident radiation interacts with electrons within the scintillating materials, allowing for the events as mentioned in sections 1.2 and 1.3 to occur. The resulting photon is released as visible light and then enters a photocathode, where electrons proportional to the number of photons entered are released. Sets of High-Voltage (HV) dynodes then amplify these



Figure 5: Image of the scintillation detector used for gamma ray spectroscopy. Present are two radiation sources, isotopes Cs-137 and Co-60, by the detector, which is also coupled with a lead shield and a base to set the radioactive materials.

electrons via secondary emissions. By the end, an anode picks up a voltage source that has more than a million more electrons than the original signal [7].

#### 3.2 Apparatus

**Figure 5** is an image of the scintillation detector used for the gamma ray spectroscopy. A 2 in. by 2 in. thallium-doped (TL) sodium iodide (NaI) crystal (*a.k.a.*, NaI(TL)) act as the detector’s base, her-

metically sealed to prevent damage since NaI (TL) is hydroscopic. The base of the detector can be seen shrouded by a lead shield, protecting the crystal from sending signals from background radiation.

The cylindrical metal tube on top of the base is the PMT. The last component is an ORTEC digibase controller, an electronic component that contains an HV source, amplifier, Pulse Height Analyzer (PHA), and a digital MultiChannel Analyzer (MCA). This setup essentially allows light signals from a radiation source to be picked up after photomultiplication, counting them into “channels”. These channels are the energy levels that the device bins them in, so a gamma ray spectrum of a radioactive isotope is essentially a histogram.

### 3.3 Object

The explanation of the mechanics behind the scintillation detector exposes then the objective of this experiment, which is to calibrate these channels into energy units so a calibration curve may be constructed and therefore be used to experimentally identify any photopeaks amongst other within a gamma ray spectrum.

The digibase, in what is called a conversion gain, has two adjustable settings: a course gain and a fine gain. The course gain is actually the set channels that the device bins the counts of photoevents in— it cannot be adjusted through the provided MAESTRO software in the laboratory. Adjusting the course gain can only be achieved by physically dismantling the digibase and changing an internal switch within its electronics. For the purpose of this experiment, the default setting of the course gain was left as is, which sets the spectrum to 1024 channels. The fine gain setting is accessible to MAESTRO, allows shifting of the channels to specific energy levels— The procedure regarding the extensive adjustment of this setting is explained more in the next section.

### 3.4 General Procedure

With the digibase connected to a Radiation Lab computer via USB-B cable, the MAESTRO software that was already downloaded and present within the laboratory computer was opened. From the menu, the MCA settings were accessed, and first the HV setting was set to a range of 800V-900V. The fine gain under the amplifier tab of the setting was initially set to 1.0 as a benchmark, but ultimately was kept for the rest of the experiments featured in this paper.

A radiation source may be placed on top of the panel inserted in a shelf level as seen in **Figure 5**. MAESTRO software provides basic spectroscopy feature such as searches for Regions of Interests (ROI), changes in window width, *etc.*, but ultimately the software was used to just collect the count data amongst the 1024 channels for later analysis in Python. Generally, data collection lasted for approximately one hour for each experiment unless otherwise specified by the lab manual. For data exporting, MAESTRO supports several formats, none which however are typical standard file extensions (*e.g.*, .csv. .xlsx, *etc.*) Out of all possible file extensions offered, .spe was found to be openable as a plain .txt file, so it was settled as the file extension to export the data.

## 4 Data Analysis

All code written to produce graphs and perform data analysis can be found within **Appendix B: Full Code Written for Analysis**.

### 4.1 Source Distance on Resolution

**Figure 6** shows an overlaid spectroscopy graph of various data gathered on Cobalt-60 (Co-60) for a given shelf level underneath the scintillator. It can be considered reasonable to guess that for equal time lapses of 1 hr for data collection, the distance between the radiation source and the scintillator is

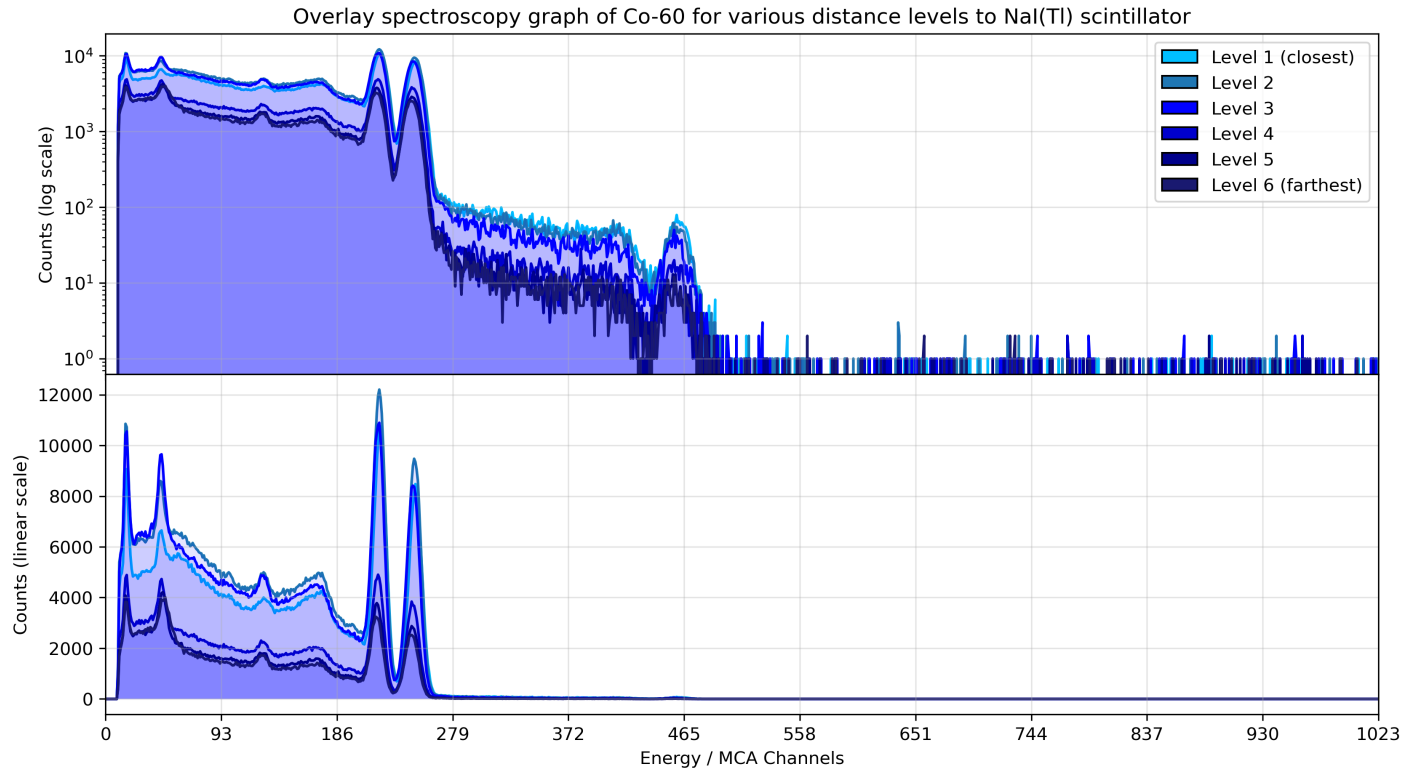


Figure 6: Overlay gamma ray spectroscopy of 6 different data gathering on source distance.

inversely proportional to the counts obtained (*i.e.*, the farther away the sample is, the less event that can be detected by the scintillator). However, it can be seen that **Figure 6** does not follow that ansatz, though this is likely due to inexact timing in time elapsed for each trial (an observer would sometime mistime when to stop data collection, so some of these trials are either under or over 1 hr of data collection).

Ultimately though, the count decrease, whether capable of being explained or not, does not effect the rest of the experiments featured in this paper, for the resolution effect that it seems to have is just vertical shifts in the spectrum position. This essentially means that a source distance away from the scintillator does not effect determinination of peaks within the graphs.

#### 4.2 Calibration

**Figure 7** displays the gamma ray spectroscopy of Cesium-137 (Cs-137) and Co-60. The typical photo-

peaks of various radioactive materials can be derived, if not searchable. This paper references the energy levels corresponding to the typical photopeaks of Cs-137 and Co-60 as being 661.6 keV, 1173.2 keV, and 1332.5 keV, respectively, where the last two values belong to Co-60 for its twin photopeaks [?].

The position of these photopeaks are determined as any number among the 1024 possible energy channels, where open-source Python packages (**scipy**) may be used to easily determine those peak positions. Given known theoretical values on the energy levels corresponding to these photopeaks, and experimentally derived energy channels corresponding to the photopeak positions, a calibration curve can be constructed to essentially convert energy channels to keV. **Figure 8** showcases a weighted linear least-squares fitting done on these three essential data points.

The acquisition of this calibration line is crucial, as it now allows radiation studies to extend to other radiation samples, whether it is known or even

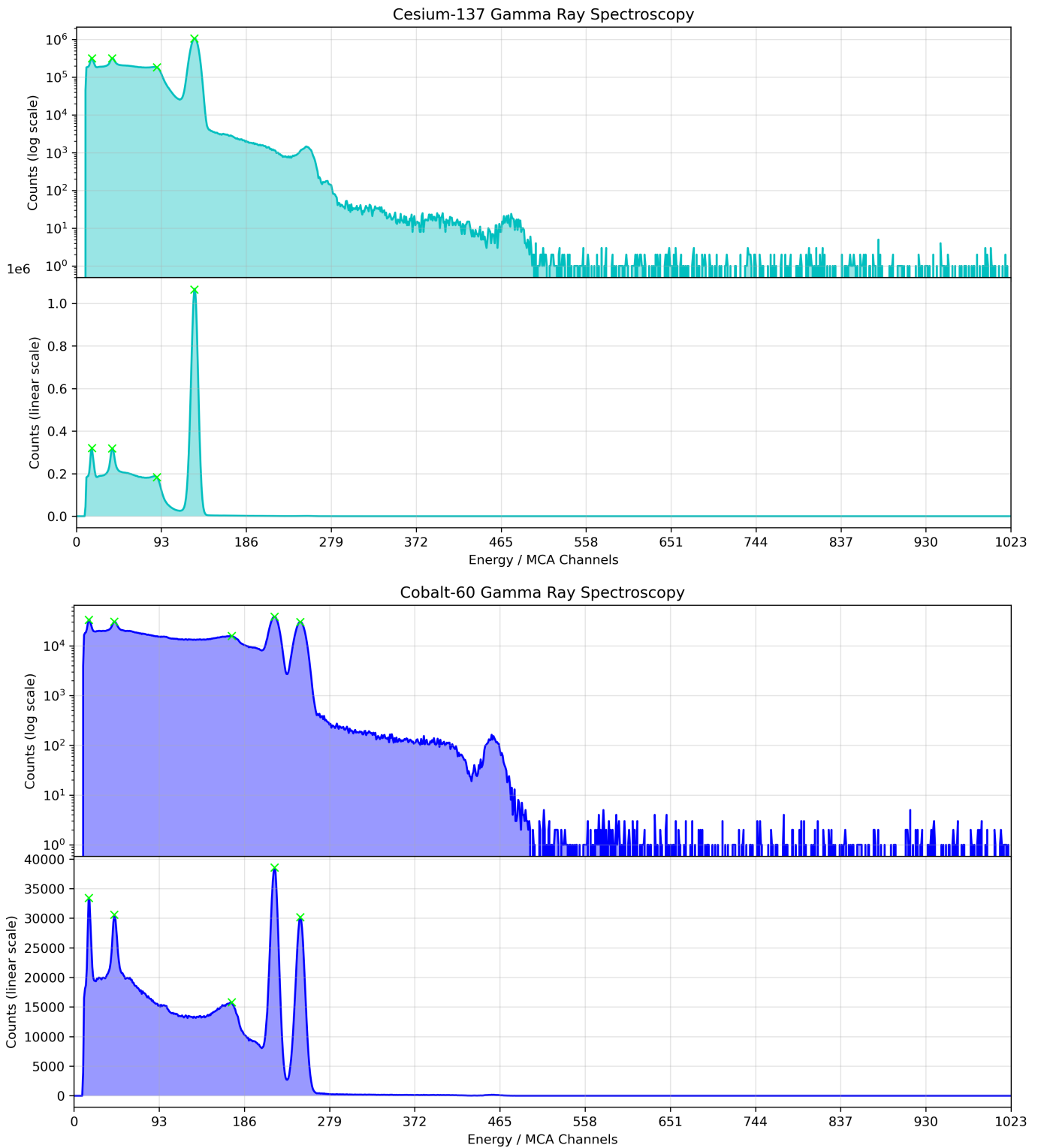


Figure 7: Calibration gamma ray spectra of Cs-137 and Co-60. Green markers represent peaks found.

unknown. This paper decides to showcases a few of these opportunities via two forms: (1) identification of an unlabeled (and therefore unknown) radiation sample found within the laboratory; and (2)

Gaussian curve fitting for various known identifiable peaks for Na-22.

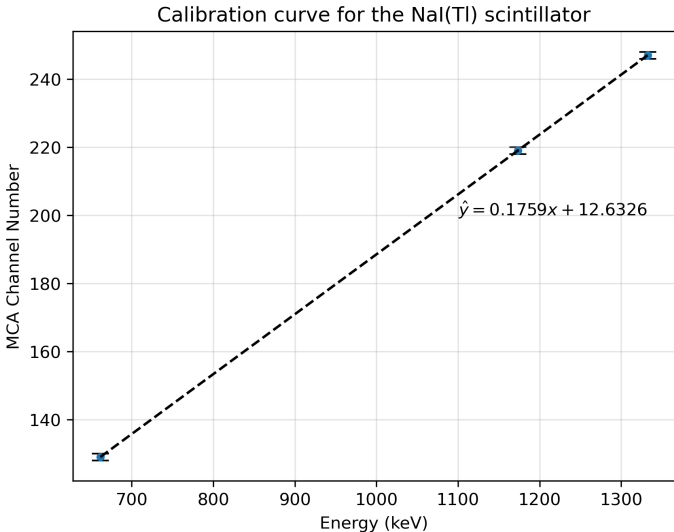


Figure 8: Calibration curve constructed using weighted linear least-squares fitting with known photopeak energy levels and experimentally determined photopeak position channel numbers.

### 4.3 Sample Identification

**Figure 9** shows the gamma ray spectrum of said unlabeled radiation sample found within the laboratory. It is at this point worth mentioning the probable order of peak type appearances in order of having the least of energy to the most: (1) X-rays; (2) annihilation; (3) backscatter; (4) Compton edge; and (5) photoelectric. Not all sample may have the first two type of peaks, as **Figure 7** showed that Cs-137 and Co-60 likely do not have annihilation peaks (it will be shown soon that Na-22 has one, which its count outweighs the rest of the type of peaks). By that note, typically then the highest peak would represent the photopeak, and given known photopeak energy levels from various radiation sources this unknown radiation sample can be identified.

From the determined channel number 132 as the position of the photopeak, the predictive line fit model converts this number to approximately 35.850 keV. From references, this result aligns with the lowest listed photopeak energy level, 35.5 keV, which belongs to Antimony-125 (Sb-125) [?]. A percent error calculation can be carried out between these two

values, but it is more notable to mention that the overestimation in converted energy level is due to the position of the found photopeak position (notice how it is marked slightly to the right of the peak in **Figure 9**), and in considering this explanation, it is then well-supported to identify the unknown sample as Sb-125.

### 4.4 Gaussian Curve Fitting

**Figure 10** shows the gamma ray spectroscopy of Na-22. Six peaks can be identified as, from left to right, X-ray lines (two of them), the annihilation curve, backscatter, Compton edge, and a photopeak. If these peaks are isolated (usually by an ROI finder) at the center of the found peak location channel number, a statistic method known as *Markov Chain Monte Carlo (MCMC)* may be carried out to probabilistically fit the most ideal Gaussian curve to the data out of various sample runs. This can be done through another open-sourced Python package (*pymc*), which allows users to build Bayesian models to fit using MCMC.

**Figure 11** shows the result of the MCMC method for fitting Gaussian curves. It can be seen that for the X-ray peaks, the model performs poorly, but is likely explained to be due to the noise to opposite sides of each peak, incorrectly shifting the prediction curves towards the noise. For the rest of the curves, however, it can be qualitatively assessed to be good fits for the measurement points gathered. It is mostly surprising that the model was able to fit the Compton edge well, for it can be seen from **Figure 10** that its peak also has elevated counts toward one side of its curve (like the X-rays).

The result of this analysis technique is incredibly useful for the capabilities of being able to find some values for the *true* parameters of a peak energy level from experimental measurements through the robust methods of counting statistics.

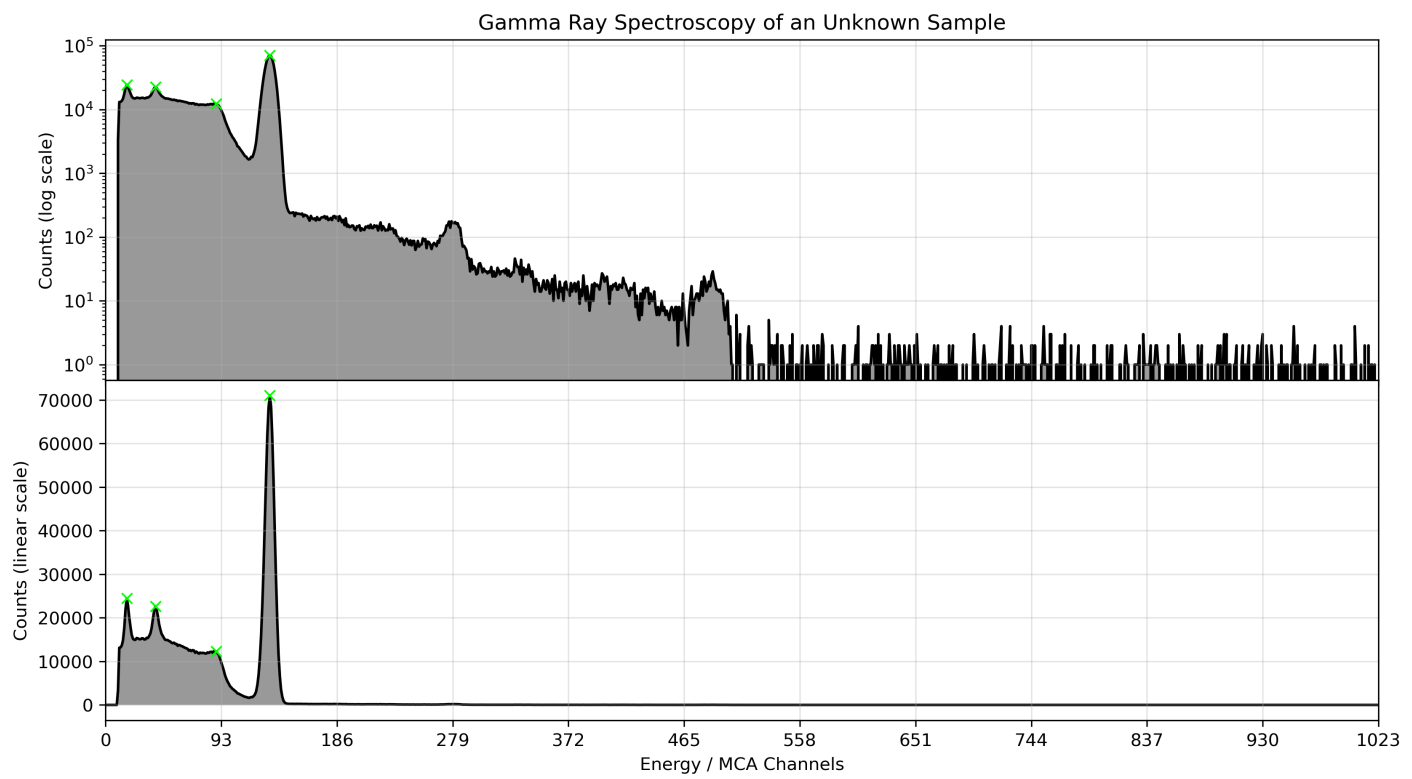


Figure 9: Gamma ray spectroscopy of an unlabeled radiation sample.

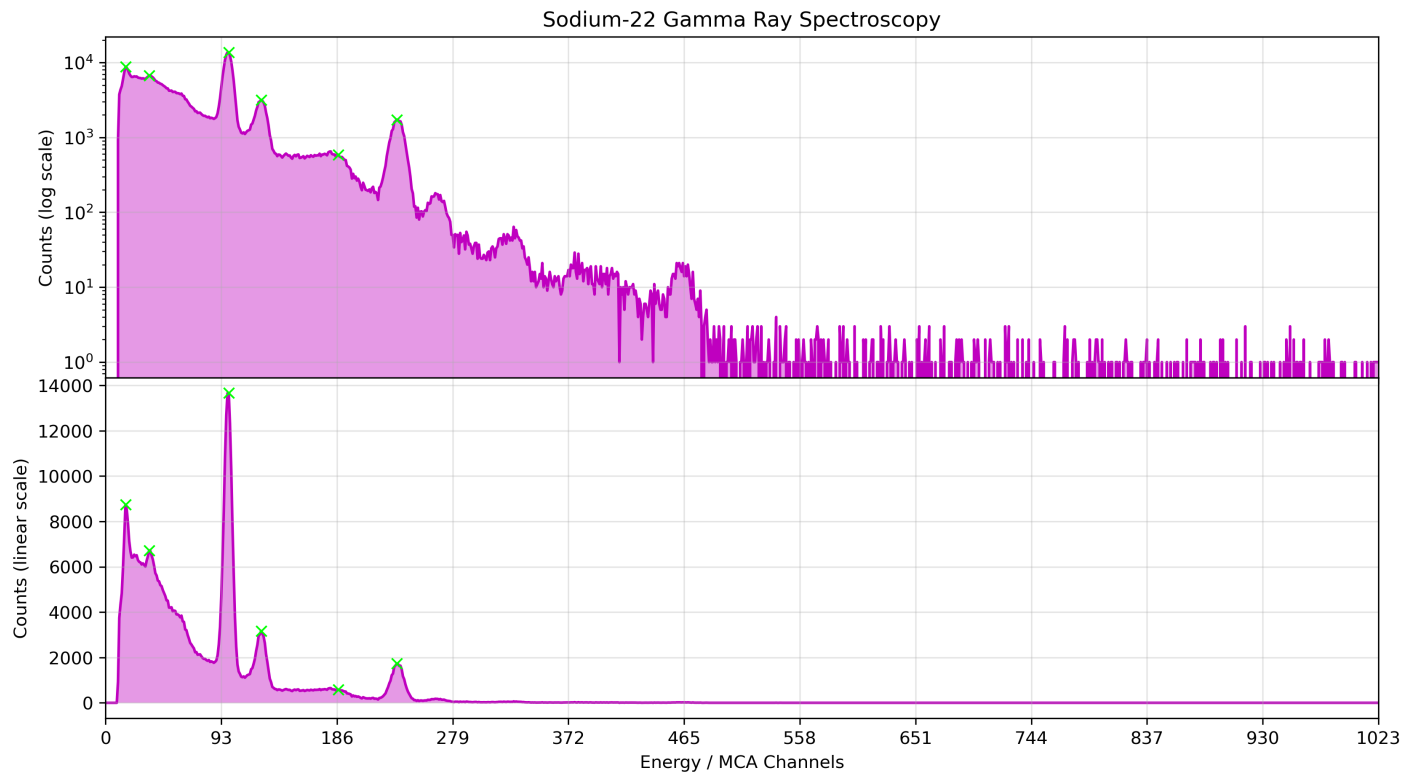


Figure 10: Gamma ray spectroscopy of Na-22.

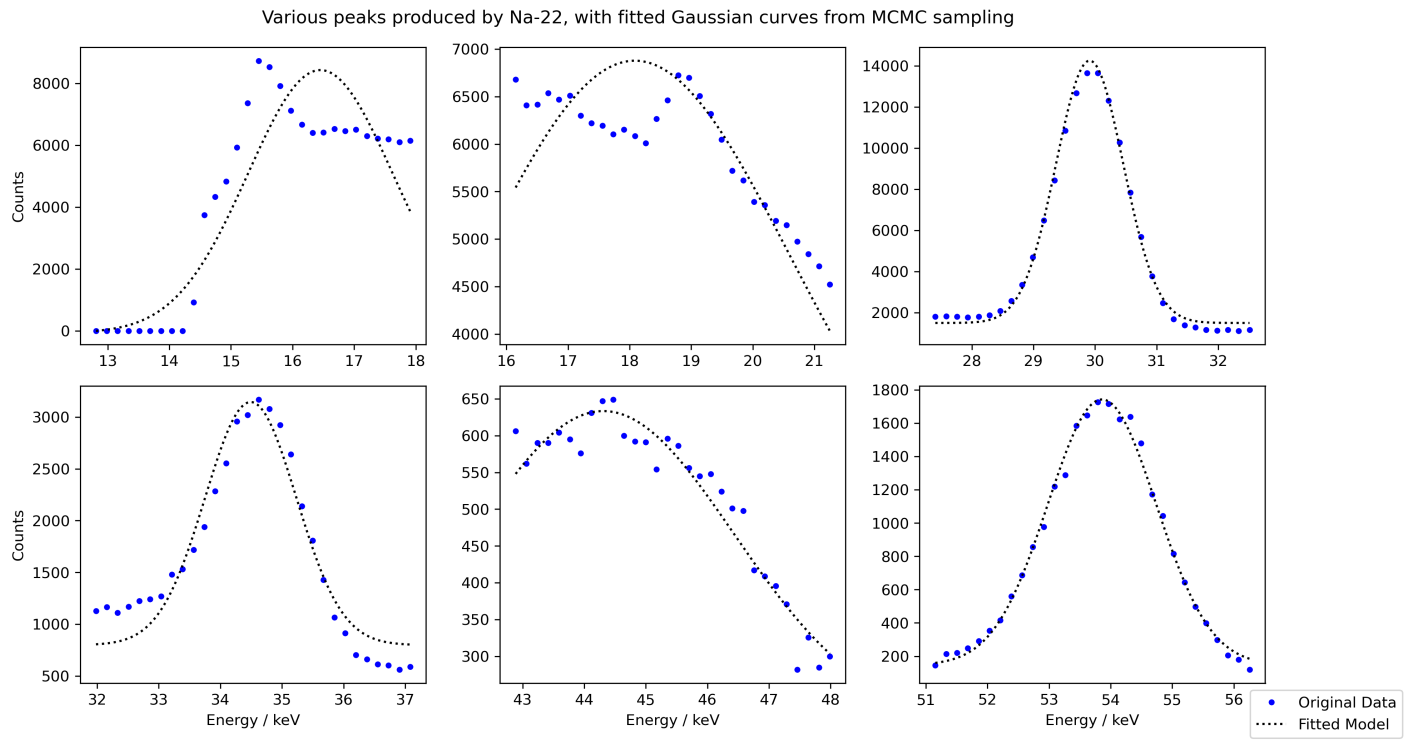


Figure 11: Gaussian curve fitting of six known peaks of Na-22 from pymc's sampling using MCMC methods and Bayesian statistics.

## References

- [1] Nuclear Security & Safeguards Education Portal, “01-Basic Radiation Detection: Introduction to Radiation Detection”, *YouTube* (2017), <https://youtu.be/y3UYdRJWacU?si=eN2ugshfn0tzByx>
- [2] Nuclear Security & Safeguards Education Portal, “21-Basic Radiation Detection: Gamma ray spectroscopy, part 1”, *YouTube* (2017), <https://youtu.be/y3UYdRJWacU?si=eN2ugshfn0tzByx>
- [3] Francesco Sciacca, Photoelectric effect, *Radiopedia* (Last revised on 29 Oct. 2024), <https://radiopedia.org/articles/photoelectric-effect>
- [4] Francesco Sciacca, Compton effect, *Radiopedia* (Last revised on 29 Oct. 2024), <https://radiopedia.org/articles/compton-effect>
- [5] Raymond Chieng, Pair production, *Radiopedia* (Last revised on 16 Jun. 2023), <https://radiopedia.org/articles/pair-production>
- [6] Nuclear Security & Safeguards Education Portal, “23-Basic Radiation Detection: Gamma: Scintillation Detectors”, *YouTube* (2017), [https://www.youtube.com/watch?v=\\_IqxMYmZe6s](https://www.youtube.com/watch?v=_IqxMYmZe6s)

## Appendix A: Derivation of the Compton Scattering Formula

- (1) We are interested in expressing a formula for the final kinetic energy of a photon in terms of its initial kinetic energy before and after the Compton Effect. Begin with the final kinetic energy of a photon and the definition of photon energy

$$E'_\gamma = hf'$$

where  $h$  is Planck's constant and  $f$  is the wave frequency. Use the frequency-wavelength relationship  $c = \lambda f$  to express the equation as

$$E'_\gamma = \frac{hc}{\lambda'}$$

- (2) At the right-hand side, introduce  $\lambda$  in the denominator via addition and subtraction

$$E'_\lambda = \frac{hc}{\lambda' + \lambda - \lambda}$$

define  $\Delta\lambda \equiv \lambda' - \lambda$  the wavelength difference between the two energy states

$$E'_\gamma = \frac{hc}{\Delta\lambda + \lambda}$$

- (3) We would like at the end to be able to express in terms of energy via  $E = hf$ , so the  $hc$  term at the right must be algebraically expressed as  $hf$  instead. Divide the numerator and denominator respectively with  $\lambda$

$$E'_\gamma = \frac{\frac{hc}{\lambda}}{\frac{\Delta\lambda + \lambda}{\lambda}}$$

the numerator is just the initial kinetic energy of the photon  $E_\gamma$ . Linearly divide  $\lambda$  in the denominator

$$E'_\gamma = \frac{E_\gamma}{1 + \frac{\Delta\lambda}{\lambda}}$$

- (4) Use the Compton Shift formula  $\Delta\lambda = \lambda_c(1 - \cos(\theta))$

$$E'_\gamma = \frac{E_\gamma}{1 + \frac{\lambda_c}{\lambda}(1 - \cos(\theta))}$$

where  $\lambda_c$  is the Compton wavelength of an electron. Express  $\lambda_c$  in terms of fundamental constants  $\lambda_c = \frac{h}{m_e c}$ , where  $m_e$  is the mass of the electron

$$E'_\gamma = \frac{E_\gamma}{1 + \frac{h}{\lambda} \frac{1}{m_e c} (1 - \cos(\theta))}$$

- (5) Multiply  $\frac{h}{\lambda}$  by  $c$  and divide  $\frac{1}{m_e c}$  by  $c$  (this does not change the overall equation since  $\frac{c}{c} = 1$ )

$$E'_\gamma = \frac{E_\gamma}{1 + \frac{hc}{\lambda} \frac{1}{m_e c^2} (1 - \cos(\theta))}$$

where  $\frac{hc}{\lambda}$  the initial kinetic energy of the photon  $E_\gamma$  appears again

$$E'_\gamma = \frac{E_\gamma}{1 + \frac{1}{m_e c^2} E_\gamma (1 - \cos(\theta))}$$

- (6) The rest energy of an electron is given by the mass-energy equivalence relation  $E_e = m_e c^2$ . Use fundamental constant values  $m_e = 9.1094 \times 10^{-31}$  kg,  $c = 2.9979 \times 10^8$  m/s and the conversion factor 1 MeV/c =  $5.344 \times 10^{-22}$  kg · m/s to finally get

$$E'_\gamma = \frac{E_\gamma}{1 + 1.96 \text{ MeV } E_\gamma (1 - \cos(\theta))}$$

where  $1.956859003$  MeV  $\approx 1.96$  MeV was approximated.

■